Temperature dynamics of a proglacial stream: Identifying dominant energy balance components and inferring spatially integrated hydraulic geometry

Jan Magnusson,[1] Tobias Jonas,[1] and James W. Kirchner[2,3]

Received 14 September 2011; revised 29 March 2012; accepted 22 April 2012; published 9 June 2012.

[1] Proglacial fields typically have complex topography and heterogeneous sediments, resulting in highly variable flow and temperature regimes in surface runoff and groundwater. Using data from the Damma glacier forefield (Switzerland), we examined how longitudinal stream temperature changes can be used to infer reach-averaged hydrological and thermal processes in proglacial riparian zones. A simple energy balance showed that (1) radiative forcing and frictional warming largely explained the observed temperature patterns in three stream reaches, and that (2) groundwater inflow and/or hyporheic exchange appear to influence stream warming along a fourth reach. Daytime stream warming depends on channel width, and here we show that stream temperature measurements can be used to infer reach-averaged hydraulic geometry relationships between stream width and discharge, which are normally difficult to obtain by other methods in braided gravel bed streams. Our results illustrate how proglacial stream temperatures can yield spatially integrated information about hydrological and thermal processes in glacial forefields, where extreme spatial heterogeneity makes conventional methods difficult to apply.

Citation: Magnusson, J., T. Jonas, and J. W. Kirchner (2012), Temperature dynamics of a proglacial stream: Identifying dominant energy balance components and inferring spatially integrated hydraulic geometry, *Water Resour. Res.*, *48*, W06510, doi:10.1029/2011WR011378.

1. Introduction

[2] Temperatures influence many biological, physical and chemical variables in streams, including chemical reaction rates [*Gooseff et al.*, 2005], distributions and growth rates of aquatic organisms [*Caissie*, 2006], water quality variables such as dissolved oxygen [*Webb et al.*, 2008], and the viscosity of water itself, which influences streambed infiltration rates in "losing" reaches [*Constanz*, 1998]. Therefore, it is important to understand the factors regulating stream temperatures and to anticipate how temperature dynamics may respond to environmental changes. In this study, we use stream temperatures and meteorological observations to investigate the factors controlling temperature dynamics along individual reaches in a braided proglacial stream.

[3] Proglacial stream temperatures typically display a fast response to meteorological forcing, with large increases in temperature over short distances downstream [*Uehlinger et al.*, 2003; *Brown and Hannah*, 2008]. These temperature increases can result from heat fluxes at the stream surface and through the streambed [*Brown et al.*, 2006; *Cadbury et al.*, 2008], and depend on the width and depth of the channel as well as the flow velocity of the water [*Chikita et al.*, 2010; *Leach and Moore*, 2011]. These observations suggest that one can potentially use measurements of longitudinal variations in stream temperature to infer how, for example, stream width varies as a function of discharge, or how stream water-groundwater interactions influence the temperature dynamics of the stream.

[4] In many studies, stream-groundwater interactions have been inferred from temperature measurements in the stream or streambed [e.g., *O'Driscoll and DeWalle*, 2006; *Westhoff et al.*, 2007; *Vogt et al.*, 2010; *Westhoff et al.*, 2011]. These methods may yield spatially integrated stream-groundwater exchange rates along whole reaches [*Becker et al.*, 2004]. Proglacial valleys are characterized by highly heterogeneous soils and stream channels, and consequently one may expect that stream-groundwater exchange will be highly localized. Thus spatially integrated measurements, such as those provided by temperature measurements at the reach scale, may be particularly useful in these settings. Conventional methods such as differential discharge measurements [*Ruehl et al.*, 2006] may not be suitable in complex, often braided, proglacial channels. Similarly, measuring temperature profiles in the streambed [*Stonestrom and Blasch*, 2003] may be impractical because it is very hard to install the sensors in the stony sediments.

[5] Stream temperature variations may help in characterizing stream properties such as channel width. The hydraulic geometry of channels is conventionally determined by direct

[1]WSL Institute for Snow and Avalanche Research SLF, Davos Dorf, Switzerland.
[2]Swiss Federal Institute for Forest, Snow, and Landscape Research, WSL, Birmensdorf, Switzerland.
[3]Department of Environmental Sciences, Swiss Federal Institute of Technology, ETH, Zürich, Switzerland.

Corresponding author: J. Magnusson, WSL Institute for Snow and Avalanche Research SLF, Flüelastr. 11, Davos Dorf, CH-7260 Switzerland. (magnusson@slf.ch)

0043-1397/12/2011WR011378

measurements across a range of flows. However, on proglacial fields, the average stream width along a reach can be very difficult to measure manually, because channel cross sections often vary greatly over short distances [*Ashmore and Sauks*, 2006]. Since channel geometry exerts a first-order influence on the energy balance of a stream, however, it may be possible to infer reach-averaged stream width from diurnal temperature dynamics, as we show below.

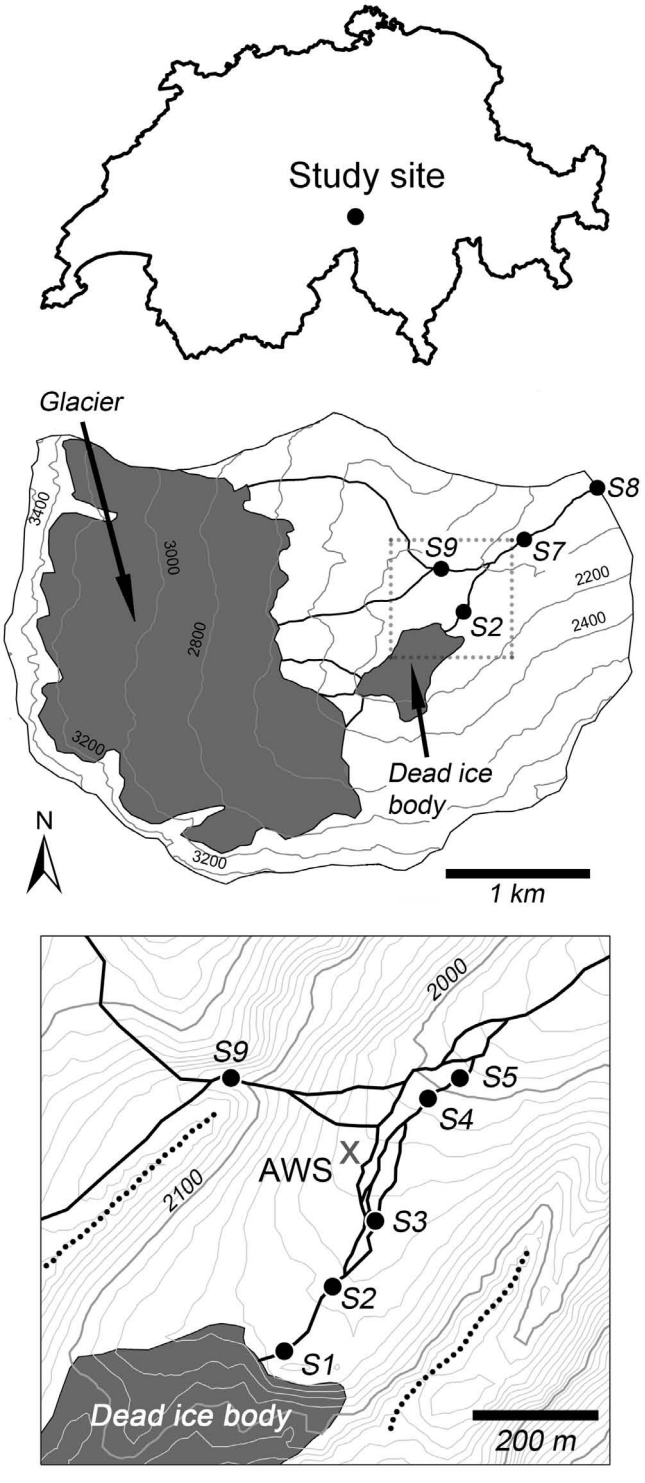

Figure 1. (top) The location of the field site, (middle) the Damma glacier watershed, and (bottom) its proglacial field in central Switzerland. The glacier forefield is bounded by a dead ice body and two large moraines from the Little Ice Age (black dotted lines in the lower map). The temperature measurement sites (S1, S2, S3, S4, S5, S8, and S9) are located along the stream emerging from the dead ice body and the stream draining the north-western part of the catchment. At three of the sites, groundwater stage and temperature were measured in monitoring well transects perpendicular to the stream (sites S1, S3, and S5). The three discharge gauging sites are located such that they measure the water flowing in from the north and south (sites S9 and S2, respectively) and out of the forefield (site S7). The automatic weather station (AWS) is situated in the middle of the proglacial field.

[6] In this study, we use temporal and spatial patterns of stream temperature and discharge in the Damma glacier forefield in the central Swiss Alps to (1) draw inferences about the energy balance of the stream, (2) calculate variations of stream width as a function of discharge, and (3) identify the thermal influence of stream-groundwater interactions from observations of longitudinal stream warming. We present an energy balance model describing the downstream temperature change along our study stream. With the model, we identify the dominant thermal and hydrological processes influencing the longitudinal temperature increase along four different stream reaches. The analysis shows that radiative forcing and frictional warming largely explain the temperature increase along all but one of the stream reaches. For one long reach, we use diurnal temperature dynamics to infer hydraulic geometry relationships describing the stream width as function of discharge. Along a fourth stream reach, we find a strong correlation between the hydraulic gradient in the riparian zone and the observed nighttime downstream temperature increase, which indicates that stream-groundwater interactions (groundwater inflow and/or hyporheic exchange) also influence the temperature dynamics of the stream locally.

2. Field Site

[7] The Damma glacier basin in the central Swiss Alps (N46°38.177′ E08°27.677′) covers an area of about 12 km^2 (Figure 1). The glacier forefield is bounded by two large moraines and a debris-covered dead ice body. Both moraines were created at the end of the Little Ice Age (~1850), and the dead ice body is now separated from the glacier, which has retreated further up the valley headwall. The forefield itself covers an area of about half a square kilometer and spans an elevation range of 1950 to 2050 m a.s.l. The hydrological regime of the study area is dominated by runoff from the seasonal snow cover and the glacier [*Magnusson et al.*, 2011].

[8] Water flows to the glacier forefield from two separate regions of the catchment (Figure 1). From the southwest regions seen in Figure 1, water flows to the glacier forefield from both the glacier and the dead-ice body. Melt water coming from the glacier flows over a rock face, and underneath the dead ice body, before emerging as a single stream channel on the forefield. From the area in the northwest of Figure 1, the glacier melt water first flows across a rock

face, then over a small proglacial area north of the forefield, before crossing the 1850 moraine and finally joining the mainstream in the middle of the forefield. The channels are braided, particularly above and around their confluence, and are characterized by highly variable geometries with large cobbles and boulders. The entire forefield is well above the tree line, and no large vegetation shades the streams. The granite bedrock is covered by debris and glacial till of unknown depth. The soils are mainly composed of cobbles and sand with some silt and minor amounts of clay. On average, snow covers the forefield from roughly November until the end of May, with the highest snow depths recorded in mid-April.

3. Methods

3.1. Observations of Thermal, Hydrological, and Meteorological Conditions

[9] Over one field season, from 27 June to 6 October 2009, we recorded thermal, hydrological and meteorological variables across the glacier forefield. We measured stream temperature at seven locations (S1, S2, S3, S4, S5, S8 and S9; see Figure 1) using standalone sensors, some of which measured both water level and temperature (Hobo U20 Water Level Logger, with 2 min sampling interval) and others of which measured temperature alone (Hobo Pro v2 Temp Logger, with 5 min sampling interval). The measurements were averaged to hourly values. At three of the stream monitoring locations (sites S1, S3 and S5), we also recorded groundwater levels and temperatures in pairs of fully screened monitoring wells situated along transects perpendicular to the stream channel. The distance between the stream and the near-stream monitoring wells varied from roughly 2 to 5 m; the distances from the streams to the farther wells varied from approximately 4 to 10 m. The distances separating each pair of wells ranged from about 2 to 5 m. The wells consisted of fully screened plastic tubes 6 cm in diameter, and extended to depths between 60 and 130 cm. For more details about the groundwater monitoring, see J. Magnusson et al. (Melt water driven stream and groundwater stage fluctuations on a glacier forefield (Damma gletscher, Switzerland), submitted to *Hydrological Processes*, 2012).

[10] We cross-calibrated the temperature sensors against one another by placing them together in a stirred laboratory water bath and slowly varying the temperature over the entire range observed in the streams (1–10°C). All of the sensors agreed within a range of ±0.11°C in these common bath experiments (exceeding the manufacturer's specifications of 0.20 and 0.37°C for the two sensor types). We corrected for observed constant offsets between the sensor readings; the largest correction was 0.10°C. Otherwise, no visible systematic deviations were detected between the temperature readings from the different probes over the entire temperature range.

[11] We continuously recorded discharge at three locations, to capture surface water flows into and out of the forefield: (1) at the stream draining the northwestern regions of the catchment (site S9), (2) at the stream close to the dead ice body draining the southwestern part of the catchment (site S2), and (3) downstream from the confluence of the streams, at a point that captures the complete catchment runoff (site S7). Stream stage was measured at these locations using the combined water level and temperature loggers described above (Hobo U20 Water Level Logger with 2 min sampling interval). The measured stream water levels were converted to runoffs using a stage-discharge rating curve measured by dilution gauging. The root-mean-square error between the dilution gauging measurements and the discharges obtained by the rating curve varied between 0.06 $m^3\ s^{-1}$ and 0.14 $m^3\ s^{-1}$ depending on location. In the analysis that follows, we used hourly averaged discharge values. We also measured the flow velocity in the streams on the forefield using travel-time observations of fluorescent dye tracers (duasyn and uranine). The flow velocity was determined from the centroid of the tracer concentration curve. Most of our velocity measurements (24 in total) were taken over a 90 m reach surrounding site S2. We also made several velocity measurements (6 in total) over the 700 m reach from site S2 to S7.

[12] We monitored meteorological conditions at an automatic weather station situated in the middle of the glacier forefield (Figure 1). The station recorded air temperature, relative humidity, wind speed, precipitation and solar radiation (hourly values averaged from 5 min sampling). The distance from the weather station to any point on the forefield is 350 m or less, so we believe that meteorological conditions recorded at the station are representative for the streams in the forefield.

3.2. Processes Influencing Stream Warming: Theory

[13] Here we present a simple energy balance equation to interpret the measured temperature time series. The downstream temperature change ΔT (°C) over a stream reach of length $L(m)$ and average width $w(m)$ can be described by the following equation:

$$\underbrace{\Delta T(t)}_{\text{Temperature change}} = \underbrace{\frac{Q(t)\,w(t)}{q(t)}\frac{L}{c\rho}}_{\text{Surface heat transfer}} + \underbrace{\frac{g\,\Delta z}{c}}_{\text{Frictional heating}} + \underbrace{\Delta T_r(t)}_{\text{Residual temperature change}}. \quad (1)$$

[14] Here Q (W m^{-2}) is the heat flux across the stream surface, c (J $kg^{-1}\ K^{-1}$) is the specific heat capacity of water, ρ (kg m^{-3}) is the density of water, Δz (m) is the change in altitude between the up- and downstream ends of the reach, g (m s^{-2}) is gravitational acceleration, q ($m^3\ s^{-1}$) is stream discharge and ΔT_r (°C) is the so-called residual temperature change. The first term of equation (1) can also be written in the more intuitive form $(Q\,A\,\tau)/(V\,c\,\rho)$, where A and V are the surface area and volume of the stream reach and $\tau = V/q$ is the mean residence time of water in the reach.

[15] Equation (1) explicitly predicts how temperature will change along a stream reach as a result of (1) heat transfer across the stream surface and (2) frictional heating due to dissipation of gravitational potential energy. Surface heat exchange warms or cools the stream at a rate that is

proportional to the heat flux, the length of the stream and the average width of the stream, and inversely proportional to the discharge. The second term of equation (1) assumes that the available potential gravitational energy completely dissipates into heat. The residual temperature change represents the heat fluxes which we cannot explain by surface heat exchange or frictional heating. Those additional heat fluxes include primarily groundwater advection, hyporheic exchange and heat conduction across the streambed. The stream energy balance equation assumes steady state conditions and constant discharge. For hourly averaged measurements, this assumption is reasonable for the Damma glacier forefield during fair-weather periods, but not during some periods with rainfall. Thus, we excluded periods with observed precipitation from our analysis presented below. In addition, we discarded periods with measured discharges outside (above 3.5 $m^3\ s^{-1}$) of the calibration range obtained for our stream gauging site (Site S2).

[16] In this study, we consider the following four components of surface heat exchange:

$$Q = LE + H + SW_{net} + LW_{net} \quad (2)$$

where LE (W m^{-2}) is latent heat flux, H (W m^{-2}) is sensible heat flux, SW_{net} (W m^{-2}) is net shortwave radiation and LW_{net} (W m^{-2}) is net longwave radiation.

3.2.1. Latent Heat Flux

[17] The turbulent heat fluxes were calculated following *Leach and Moore* [2010]. We estimated the latent heat flux using the parameterization below:

$$LE = 285.9(0.132 + 0.143\,u)(e_a - e_w) \quad (3)$$

where u (m s^{-1}) is the wind speed, e_a (kPa) is the vapor pressure of air and e_w (kPa) is the vapor pressure directly above the stream surface. The latter was calculated by combining the saturation pressure function [*Stull*, 2000] and the measured water temperature. The vapor pressure of air was determined by multiplying the measured relative humidity with the results obtained from the saturation pressure function using measured air temperature as input.

3.2.2. Sensible Heat Flux

[18] We estimated the sensible heat flux by scaling the calculated latent heat flux with the Bowen ratio β:

$$H = \beta LE \quad (4)$$

where β is given by

$$\beta = 0.66(p/1000)\,[(T_w - T_a)/(e_w - e_a)] \quad (5)$$

and $p(kPa)$ is the air pressure, T_w (°C) is the stream water temperature and T_a (°C) is the air temperature. Air pressure was set constant to 80.3 kPa.

3.2.3. Shortwave Radiation

[19] The net shortwave radiation SW_{net} was calculated with the water albedo α (*dimensionless*) and the measured incoming shortwave radiation SW_{in} (W m^{-2}) as

$$SW_{net} = (1 - \alpha)SW_{in} \quad (6)$$

[20] The water albedo was fixed at 0.05 [*Leach and Moore*, 2010].

3.2.4. Longwave Radiation

[21] The net longwave radiation LW_{net} was determined using parameterizations. The incident atmospheric radiation was calculated by combining the clear-sky algorithm of *Dilley and O'Brien* [1998] with the cloud-correction algorithm of *Unsworth and Monteith* [1975]. First, the clear-sky emissivity ε_{clr} was calculated following *Dilley and O'Brien* [1998]:

$$L_{clr} = 59.38 + 113.7\left(\frac{T_a + 273.16}{273.16}\right)^6 + 96.96\sqrt{w/25} \quad (7)$$

$$\varepsilon_{clr} = L_{clr}/(\sigma(T_a + 273.16))^4 \quad (8)$$

where L_{clr} (W m^{-2}) is clear-sky longwave radiation and w (cm) is precipitable water given by $w = 4650e_a/(T_a + 273.16)$. Second, we estimated an effective atmospheric emissivity ε_a using the cloud-correction proposed by *Unsworth and Monteith* [1975]:

$$\varepsilon_a = (1 - 0.84c_{cloud})\varepsilon_{clr} + 0.84c_{cloud} \quad (9)$$

where c_{cloud} is the fraction of cloud cover, which we estimated by comparing the measured solar radiation with the clear-sky radiation following *Campbell* [1985]. Finally, incoming longwave radiation was estimated using the Stefan-Boltzmann radiation law and the calculated effective atmospheric emissivity. This combination of parameterizations was shown to give reliable predictions of incoming long-wave radiation for our study site [*Magnusson et al.*, 2011]. For more details, see *Flerchinger et al.* [2009] who summarized the methods we used. Outgoing longwave radiation was determined from the measured stream temperature using the Stefan-Boltzmann radiation law. The emissivity of water was set constant to 0.95 [*Leach and Moore*, 2010].

3.3. Processes Influencing Stream Warming: Identify Dominant Processes

[22] With the energy balance equation described above, we analyzed whether heat transfer across the stream surface, frictional warming or the residual temperature change dominated the longitudinal temperature increase observed over four stream reaches delineated by our monitoring sites (site S1 to S2, S2 to S3, S3 to S4, and S4 to S5). To assess the importance of surface heat transfer, we plotted the observed downstream change in stream temperature (ΔT on the vertical axis) as a function of the calculated heat flux across the stream surface divided by discharge (Q/q on the horizontal axis). The slope of the regression line describes the relationship between the average stream width, the stream length, the specific heat of water and the density of water ($Lw/c\rho$ in equation (1)). This slope is not constant because the stream width varies as a function of discharge. For this reason, we performed the regression analysis within three discharge categories ($0.6 < q < 0.9$ $m^3\ s^{-1}$; $1.1 < q < 1.7$ $m^3\ s^{-1}$; $2.1 < q < 3.3$ $m^3\ s^{-1}$). The intercepts of the regression lines indicate the influence of

frictional warming ($g\Delta z/c$). We treat the residual temperature change as an error term, which likely would disturb the linear relationship between the temperature increase (ΔT) and the heat transfer across the stream surface divided by discharge (Q/q). In the case of a substantial residual temperature change, the intercept of the regression line may also no longer equal the contribution by frictional warming ($g\Delta z/c$). Note that we report the regression results (the slopes and intercepts) by regressing Q/q on ΔT and inverting the resulting linear equations, because the scatter in the relationships between ΔT and Q/q arises mostly from uncertainties in Q/q rather than ΔT [*Smith*, 2009].

3.4. Inferring Hydraulic Geometry Relationships From Stream Temperature Measurements

[23] The stream energy balance indicates that the longitudinal temperature increase over a stream reach depends on stream width (see equation (1)). Thus, observations of stream warming along a reach represent indirect measurements of stream width, which may be helpful in estimating reach-averaged hydraulic geometry relationships in irregular channels such as ours. The three basic hydraulic geometry relationships express width, depth, and velocity as power functions of discharge [*Leopold and Maddock*, 1953; *Park*, 1977]:

$$Width = aq^b \tag{10}$$

$$Depth = cq^f \tag{11}$$

$$Velocity = kq^m \tag{12}$$

where the product of the coefficients ($a \cdot c \cdot k$) and the sum of the exponents ($b + f + m$) should be equal to one [*Park*, 1977]. We can estimate the relationship between stream width and discharge by two independent methods, both based on the stream energy balance equation (equation (1)).

[24] In the first method, we rewrite equation (1) to obtain an expression for the stream width

$$w(t) = \frac{q(t)c\rho}{Q(t)L}\left(\Delta T(t) - \frac{g\Delta z}{c} - \Delta T_r(t)\right) \tag{13}$$

in which all terms except the channel width $w(t)$ and the residual temperature change ΔT_r can be directly measured or calculated (note that here, c is the specific heat of water rather than the hydraulic geometry constant in equation (11)). For the stream width calculations, we estimated the residual temperature change by (1) determining the intercept of the regression lines between Q/q and ΔT for discharges within decile ranges (i.e., the lowest 10% of flows, the next 10% and so forth), (2) subtracting the contribution of frictional warming from those intercepts, and (3) fitting a parametric function through those points as a function of discharge. We assumed that this parametric function described the residual temperature change. In addition, we restricted our calculations using equation (13) to periods when the calculated net surface heat flux $Q(t)$ exceeded 700 W m^{-2}, so that shortwave radiation dominates the energy balance, and the fractional uncertainty in $Q(t)$ is relatively small.

[25] In the second method, we directly infer the stream width from the slope of the regression line between longitudinal warming (ΔT) and surface heat flux per unit discharge (Q/q) within narrow ranges of discharges. The slope, denoted s_{heat} in the following, equals the relationship between the stream length and width in relation to the heat capacity and density of water ($Lw/c\rho$ as seen in equation (1)). Therefore, one can infer the average stream width in a narrow range of discharge from the slope s_{heat}:

$$w = s_{heat}\frac{c\rho}{L} \tag{14}$$

[26] Consequently this method does not require any knowledge about residual temperature changes within the reach (compare equation (13) and (14)). We calculated the stream width by determining the regression slopes between ΔT and Q/q for 10 discharge bins, corresponding to the lowest 10% of flows, the next 10% and so forth similarly as described above.

4. Results

4.1. Observations of Thermal, Hydrological, and Meteorological Conditions

[27] During the study period, meteorological conditions were relatively warm and moist; the average air temperature was approximately 10°C and the relative humidity was roughly 75%. During this period, precipitation fell as rain in the forefield, but occasionally fell as snow at higher altitudes. The precipitation gauge recorded approximately 360 mm of rainfall over the study period, and during 48% of the days rainfall totaled more than 1 mm. In spite of the rather moist climate, many days were very sunny, and about half of the days (53%) during the monitoring period had at least 1 h with hourly average solar radiation exceeding 700 W m^{-2}.

[28] The observed stream temperatures displayed large variations across the glacier forefield (Figure 2, top). Low temperatures, varying between 0.7 and 4.2°C, were recorded downstream of the dead ice body (site S1) during the monitoring period. Markedly higher temperatures (Figure 2, top), varying between 0.1 and 11.4°C, were observed in the northern tributary stream as it crossed the northern large moraine (site S9). Temperatures recorded downstream of the confluence (at site S8) were intermediate between temperatures at the two upstream observation points (sites S1 and S9), ranging from 1.5 to 9.2°C during the monitoring period (Figure 2, middle). The peak-to-peak amplitudes in the diurnal temperature fluctuations at site S8 were also intermediate between the amplitudes of the two upstream measurements.

[29] Figure 3 shows that the sum of the discharges measured above the confluence nearly equaled the discharges observed below the confluence (coefficient of determination $r^2 = 0.98$, slope of regression line through origin = 0.96, root-mean-square error = 0.15 m^3 s^{-1}). The discrepancy between the discharge measurements was slightly smaller than the uncertainty in the measurements themselves.

[30] We calculated stream temperatures below the confluence (dashed line in Figure 2, middle) by combining the daily average measurements of discharge and stream temperature from the two tributaries (temperatures measured at

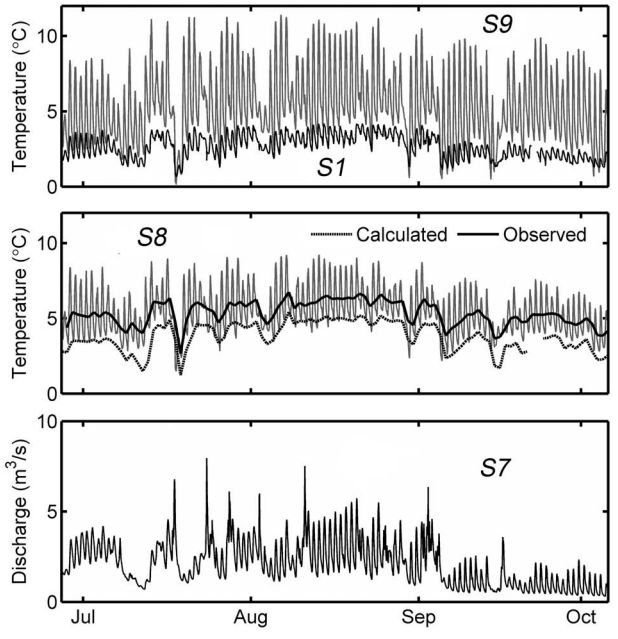

Figure 2. (top, middle) The observed hourly stream temperatures (sites S1, S8, and S9) and (bottom) discharges (site S7) show large diurnal and seasonal variations. (middle) The daily averaged stream temperature calculated by mixing the two main streams (sites S1 and S9) flowing into the forefield (dashed line) is systematically lower than the daily averaged temperature of the water leaving the forefield at site S8 (black line), and is often lower than the daily minimum temperature at S8 (gray line).

sites S9 and S1, discharges measured at sites S9 and S2). The measured daily average stream temperature below the confluence (black line in Figure 2, middle) is approximately 1.5°C higher than the calculated value. (Note that

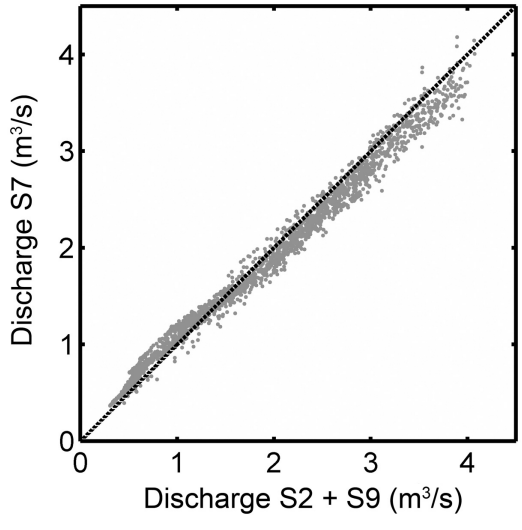

Figure 3. Stream discharge measured at the downstream gauging station (site S7), compared to the sum of measured discharges on the two main tributaries (sites S2 and S9) including the one-to-one line. The close agreement indicates that no large net gains or losses of groundwater occurred along the braided streams on the proglacial field.

streamflow velocity is high, resulting in travel times of less than 1 h from the two upstream sites to the downstream site; therefore we did not account for this short time lag in our calculations based on daily averages.)

[31] By analyzing the temperature increase along individual stream channels, we gain more information about the processes influencing the stream heating than by studying single temperature measurements. We compared three temperature measurements delineating two individual stream reaches (S2 to S4 and S4 to S5; Figure 4, top). These two reaches were selected because they display visually different diurnal patterns of temperature increases. Figure 4 (middle) shows that the temperature increase over the longer reach (S2 to S4, length = 330 m) is larger, particularly during daytime, than over the shorter reach (S4 to S5, length = 60 m). Along the longer reach, the temperature increase responded strongly to solar radiation ($r^2 = 0.92$) and less to air temperature variations ($r^2 = 0.56$). The shorter reach displayed weaker correlations with both solar radiation ($r^2 = 0.60$) and air temperature ($r^2 = 0.38$) than the longer reach did. The correlations above were determined using a cross-correlation analysis that shifted the signals in time until the strongest correlations were achieved. The differences in the correlation coefficients between the reaches show that the two time series describing the temperature increase differ in shape, which is also visually obvious in Figure 4. During nighttime, the temperature increase along the shorter reach (S4 to S5) nearly equaled that of the longer reach (S2 to S4).

4.2. Processes Influencing Stream Warming: Identify Dominant Processes

[32] For the long stream reach (S2 to S4) we find a clear relationship between the observed temperature increase and the surface heat flux (calculated with equation (2)) divided by discharge (Figure 5). One particularly interesting event occurred in the beginning of September, when stream discharge suddenly decreased after snowfall on the glacier (which raised the glacier's surface albedo and lowered its melt rate). Following this snowfall, the longitudinal warming along this reach displayed much larger diurnal fluctuations than before. Surface heat fluxes were similar before and after the snowfall event, but discharge dropped from roughly 1–4 $m^3\ s^{-1}$ to roughly 0.5–1 $m^3\ s^{-1}$.

[33] With the energy balance equation described above, we analyzed whether the heat transfer across the stream surface, frictional warming or the residual temperature change dominated the longitudinal temperature increase observed over the four stream reaches (site S1 to S2, S2 to S3, S3 to S4, and S4 to S5). We first illustrate this approach using the long stream reach stretching from S2 to S4 which shows a clear relationship between the stream warming and the surface heat fluxes per unit discharge (see Figure 5). To assess the importance of the surface heat fluxes, we plotted the observed stream warming (ΔT on the vertical axis of Figure 6) against the calculated heat fluxes across the stream surface divided by discharge (Q/q on the horizontal axis of Figure 6) for three distinct discharge categories. The surface heat fluxes per unit discharge explained 88–91% of the variance in the temperature increase. The slope of the regression line became steeper with increasing discharge (from 8.5×10^{-4} to 15.1×10^{-4} $m^5\ K\ J^{-1}$). The

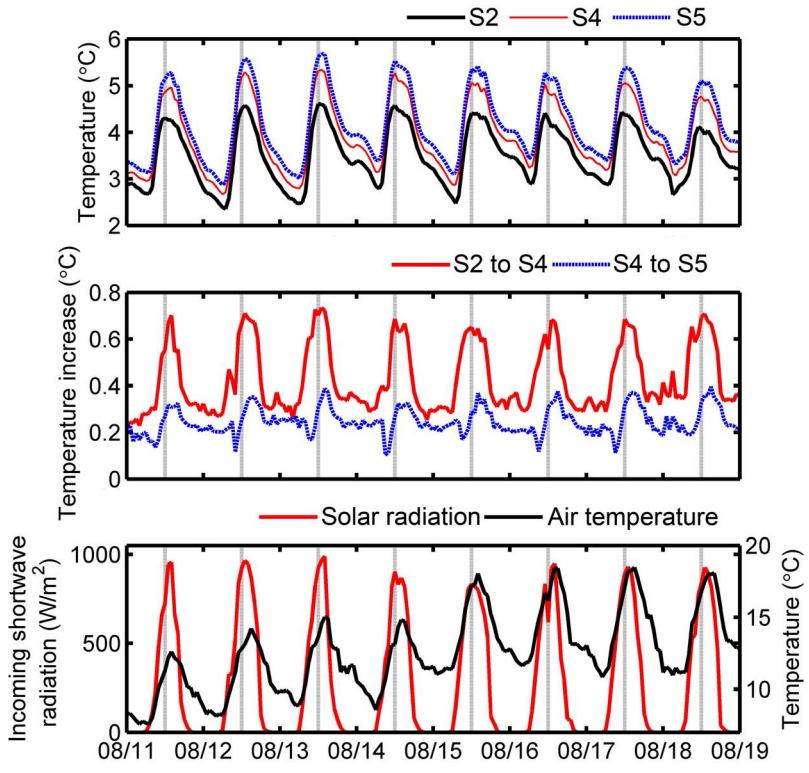

Figure 4. (top) Measured stream temperature at three locations, (middle) and the temperature increase over two individual reaches, (bottom) compared to meteorological conditions observed at the forefield. The temperature increases over the two stream reaches showed different behavior: the temperature change over the longer upstream reach (S2 to S4, Figure 4 (middle), solid red line) showed a clear response to solar radiation whereas the shorter downstream reach (S4 to S5, Figure 4 (middle), dashed blue line) displayed a weak response to variations in both air temperature and solar radiation.

observed intercept varied between 0.18 and 0.24°C depending on discharge, and exceeded the calculated frictional warming of 0.10°C.

[34] Using the method shown in Figure 6, we also analyzed the longitudinal temperature increase observed along four shorter stream reaches (Table 1). The measurements over the three upstream reaches (S1 to S2; S2 to S3; S3 to S4) displayed similar characteristics to those obtained for the long stream reach (S2 to S4) which encompasses two of those shorter reaches. In most cases, the observed longitudinal temperature increase correlated strongly with the surface heat flux divided by discharge, and the slope of the regression line always became steeper as discharge increased. The intercept approximately matched or slightly exceeded the calculated frictional warming. In contrast, the longitudinal temperature increase observed over the very short downstream reach (S4 to S5, 60 m in length) behaved differently from those observed over the upstream sections. In this short reach, the r^2 between the temperature increase and the surface heat flux divided by discharge was very low, ranging between 0.00 and 0.09. The relationship between ΔT and Q/q is too weak to give meaningful regression fits for this particular reach. However, both the average daytime (07:00 to 20:00) temperature increase of 0.25°C and the average nighttime (21:00 to 6:00) temperature increase of 0.23°C greatly exceeded the calculated frictional warming of 0.02°C.

4.3. Inferring Hydraulic Geometry Relationships From Stream Temperature Measurements

[35] For stream width calculations using equation (13), we need to estimate the contribution of the residual temperature change to the observed stream warming. Figure 7 shows how the slope and intercept of the regression line between the longitudinal temperature increase (ΔT) and the surface heat fluxes per unit discharge (Q/q) vary for a series of runoff bins, for the reach between sites S2 to S4. The intercepts of the regression lines decrease with discharge, whereas the slopes of the regression lines increase with runoff. We describe the residual temperature change with a parametric function ($\Delta T_r = 1.2 \times q^{-0.05} - 1.1$) fitted to the intercepts (after subtracting the contribution by frictional warming).

[36] Figure 8 shows the estimated stream widths for the reach from S2 to S4 inferred from individual values of ΔT and Q/q using equation (13), plotted as gray dots, together with the fitted hydraulic geometry relationship $w = 12.0 \pm 0.2\ q^{0.49 \pm 0.02}$ (uncertainties reported as ±1 standard error), shown as a black line. The individual values of the calculated stream widths are somewhat uncertain (the RMSE around the fitted curve is 1.7 m). Stream widths inferred from the regression slopes (see Figure 7) using equation (14), shown as black squares in Figure 8, lie slightly above the hydraulic geometry relationship inferred from individual

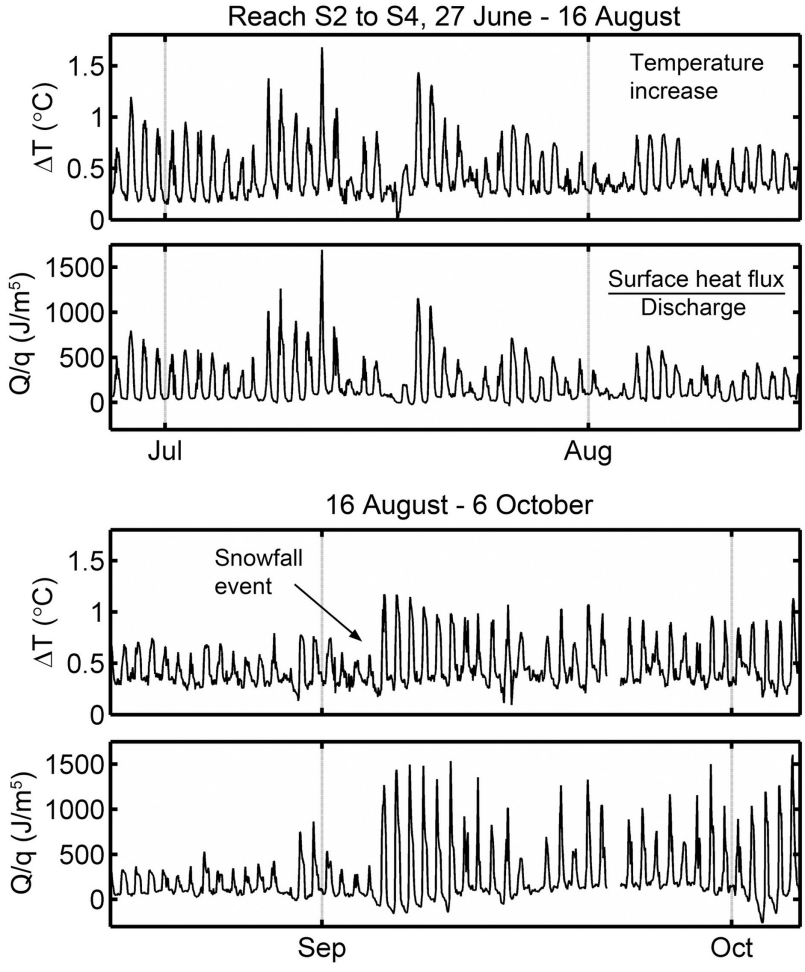

Figure 5. The observed stream temperature increase (ΔT) shows a strong relationship with the surface heat fluxes per unit discharge (Q/q) for the reach stretching from site S2 to S4. In the beginning of September, the discharge decreased abruptly but the surface heat fluxes remained high (large Q/q ratio). Due to the lower volume of water in the stream, the diurnal temperature rise was much larger than before.

values of ΔT and Q/q using equation (13). The results from both methods show a clear relationship between discharge and calculated stream width. Figure 9 shows the measured streamflow velocities as a function of discharge, together with the fitted velocity relationship $v = 0.46 \pm 0.01\ q^{0.29\pm0.04}$ (± 1 standard error). By combining the width-discharge relationship and the velocity-discharge relationship, we calculated the relationship between average depth and discharge across the study reach as $d = 0.18 \pm 0.01\ q^{0.22\pm0.05}$ (with standard errors estimated by Gaussian error propagation). Figure 10 shows this reach-averaged depth-discharge relationship with observed stream stage at the two locations along the study reach where stream level was measured (sites S2 and S3).

4.4. Processes Influencing Stream Warming: Analyzing the Stream Energy Balance

[37] In the following analysis, we investigated the observed temperature increases over the long stream reach spanning from S2 to S4, which display a strong response to meteorological forcing (Table 1 and Figure 4). Along this reach, the temperature increases almost proportionally with the surface heat fluxes, illustrated within three defined discharge ranges in Figure 11 (right). On the other hand, stream warming is inversely related to discharge within narrow ranges of surface heat fluxes (Figure 11, left).

[38] During the monitoring period, on average, all of the energy balance components were positive, making the stream water warmer (Table 2). Shortwave radiation contributed most to the average stream energy balance. The residual temperature change, given by the parametric function obtained above ($\Delta T_r = 1.2 \times q^{-0.05} - 1.1$), was the second largest term in the energy balance during daytime, and the largest term at night. Frictional warming increased the stream temperature by about 0.10°C over the reach, making a significant contribution to the stream energy balance. During the study period, air temperatures were on average 7°C higher than the stream temperatures and exceeded the stream temperatures about 98% of the time, implying positive sensible heat fluxes. Large differences between air and stream temperature, combined with high relative humidity, also resulted in positive latent heat fluxes throughout day and night. The higher air than stream temperatures furthermore is an indication of a net positive longwave radiation flux to the stream. The relative importance of different energy balance components shifts with time of day, with shortwave radiation dominating the

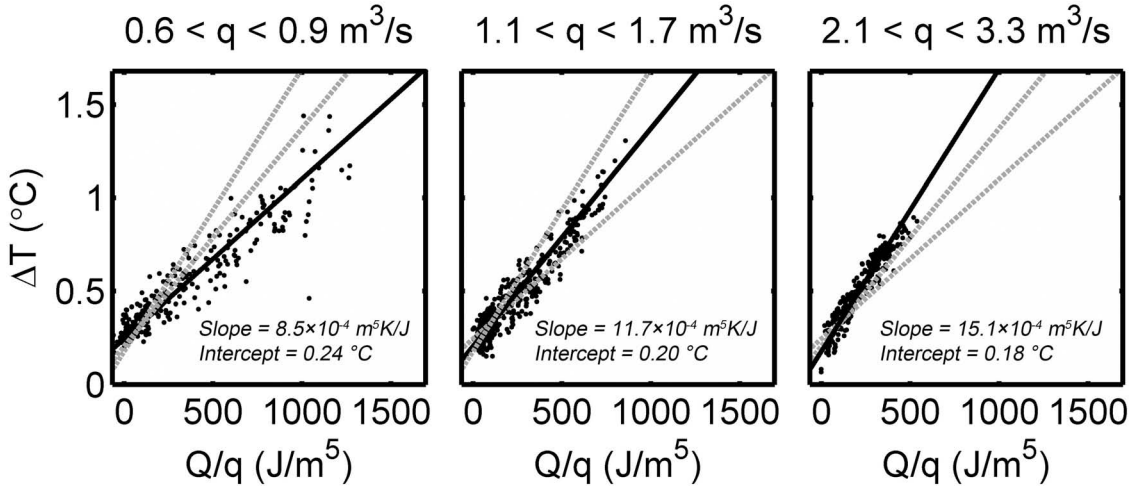

Figure 6. Observed temperature increases over the long reach stretching from S2 to S4, showing linear relationships with surface heat fluxes per unit discharge, in three ranges of discharge. The slope of this relationship increases with discharge, reflecting the increase in stream width (and thus surface area) with increasing discharge. The regression line for each discharge range is shown in black; the lines for the other two discharge ranges are shown as gray dashed lines for comparison. Note that the slopes and intercepts reported here are obtained by regressing Q/q on ΔT and inverting the resulting linear equations, because the scatter in the data is assumed to arise mostly from uncertainties in Q/q rather than ΔT.

stream warming during daytime whereas frictional warming and the residual temperature change dominate during nighttime (Table 2).

5. Discussion

5.1. Observations of Thermal, Hydrological, and Meteorological Conditions

[39] We observed large temporal and spatial variability in stream temperatures in the Damma forefield, similar to results reported in studies of other proglacial field sites [*Uehlinger et al.*, 2003; *Brown and Hannah*, 2008]. The observed stream temperatures were well above the freezing point at the location closest to the dead ice body (site S1), indicating that much of the water reaching this location was warmed as it crossed the rock face below the glacier, before passing underneath the dead ice body (see Figure 1). The even higher measured temperatures in the northern tributary stream (site S9) showed that the melt water from the glacier, which had already traveled between 1 and 2 km across an open rock face and a small proglacial area before reaching this location (see Figure 1), responded strongly to atmospheric heat fluxes during daytime. Thus, the cold glacier melt water can warm quickly (up to roughly 10°C) during daytime over short distances (less than roughly 2 km). The observed stream temperatures at the site below the

Table 1. Linear Relationships Between the Longitudinal Temperature Increase and the Heat Transfer Across the Stream Surface Per Unit Discharge, Bounded Within Defined Discharge Intervals, for Individual Stream Reaches[a]

Stream Reach	Discharge Interval ($m^3 s^{-1}$)	r^2	Slope of Regression Line ($m^5 K J^{-1}$)	Intercept of Regression Line (°C)	Calculated Frictional Warming (°C)	Length of Stream Reach (m)
S2 to S4	0.6–0.9	0.88	$8.5 \pm 0.2 \times 10^{-4}$	0.24 ± 0.01	0.10	330
S2 to S4	1.1–1.7	0.90	$11.7 \pm 0.2 \times 10^{-4}$	0.20 ± 0.00	0.10	330
S2 to S4	2.1–3.3	0.91	$15.1 \pm 0.3 \times 10^{-4}$	0.18 ± 0.01	0.10	330
S1 to S2	0.6–0.9	0.67	$4.3 \pm 0.2 \times 10^{-4}$	-0.06 ± 0.01	0.02	130
S1 to S2	1.1–1.7	0.75	$6.2 \pm 0.2 \times 10^{-4}$	-0.05 ± 0.00	0.02	130
S1 to S2	2.1–3.3	0.83	$12.6 \pm 0.4 \times 10^{-4}$	-0.04 ± 0.01	0.02	130
S2 to S3	0.6–0.9	0.79	$4.6 \pm 0.2 \times 10^{-4}$	0.13 ± 0.01	0.03	130
S2 to S3	1.1–1.7	0.63	$7.6 \pm 0.3 \times 10^{-4}$	0.05 ± 0.01	0.03	130
S2 to S3	2.1–3.3	0.64	$9.8 \pm 0.5 \times 10^{-4}$	-0.02 ± 0.01	0.03	130
S3 to S4	0.6–0.9	0.86	$4.6 \pm 0.1 \times 10^{-4}$	0.09 ± 0.01	0.07	200
S3 to S4	1.1–1.7	0.88	$6.5 \pm 0.1 \times 10^{-4}$	0.11 ± 0.00	0.07	200
S3 to S4	2.1–3.3	0.81	$9.3 \pm 0.3 \times 10^{-4}$	0.12 ± 0.01	0.07	200
S4 to S5	0.6–0.9	0.03	n/a	n/a	0.02	60
S4 to S5	1.1–1.7	0.00	n/a	n/a	0.02	60
S4 to S5	2.1–3.3	0.09	n/a	n/a	0.02	60

[a]For defined discharge intervals, see Figure 6; for individual stream reaches, see Figure 1. High r^2 values and small differences between the intercept of the regression line and the calculated frictional warming indicate reaches where stream warming is primarily controlled by surface heat fluxes. For the most downstream reach (site S4 to S5), the relationship between ΔT and Q/q is too weak to give meaningful regression fits. Note that the slopes and intercepts reported here were obtained by regressing Q/q on ΔT and inverting the resulting linear equations, because the scatter in the $Q/q - \Delta T$ relationship is assumed to arise mostly from uncertainties in Q/q rather than ΔT. Uncertainties are reported as ± 1 SE.

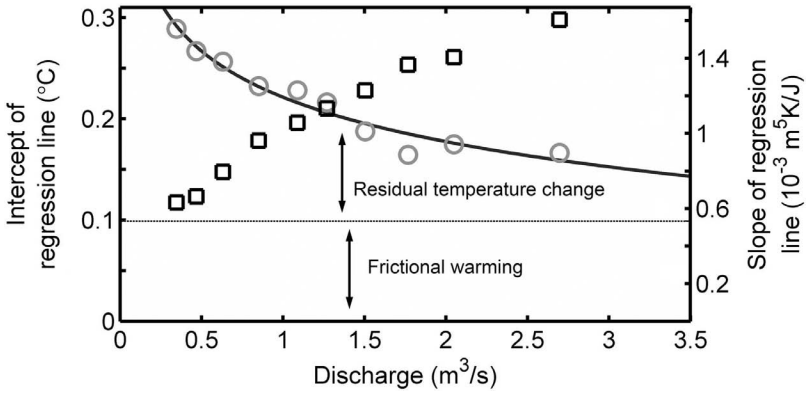

Figure 7. Slopes and intercepts (black squares and gray circles, respectively) of regression relationships between longitudinal temperature increases from S2 to S4 (ΔT) and surface heating per unit discharge (Q/q) for a series of discharge bins. The slopes of the regression lines (black squares) become steeper with increasing discharge, reflecting an increase in stream width. The regression intercepts (gray circles, with fitted black curve) indicate the increase in stream temperature with no net surface heating. They decline with increasing discharge, but always exceed the calculated frictional warming. Note that the slopes and intercepts reported here were obtained by regressing Q/q on ΔT and inverting the resulting linear equations, because the scatter in the $Q/q - \Delta T$ relationship is assumed to arise mostly from uncertainties in Q/q rather than ΔT.

confluence (site S8) were roughly 1.5°C higher than the volume-weighted average of the waters passing the two upstream measurement locations (S1 and S9). The differences demonstrate that the streams on the forefield are not in equilibrium with the surroundings, and that inferences regarding the stream's energy balance can be gathered by studying longitudinal temperature variations in the streams.

[40] We find different diurnal patterns in the temperature increases measured over two different stream reaches on the forefield (Figure 4). For the upstream reach (site S2 to S4), the stream temperatures reacted quickly to changes in meteorological conditions, and did not demonstrate any long-term memory of past variations in either solar radiation or air temperature. This is not paradoxical because cold melt water continually flushes the system quickly, resulting in residence times shorter than one solar heating cycle. The strong correlation between the temperature increase and shortwave radiation along the upstream reach suggests that direct solar heating is an important process warming the stream. The temperature increase along the short downstream reach (site S4 to S5) was relatively large during nighttime, particularly compared to the longer

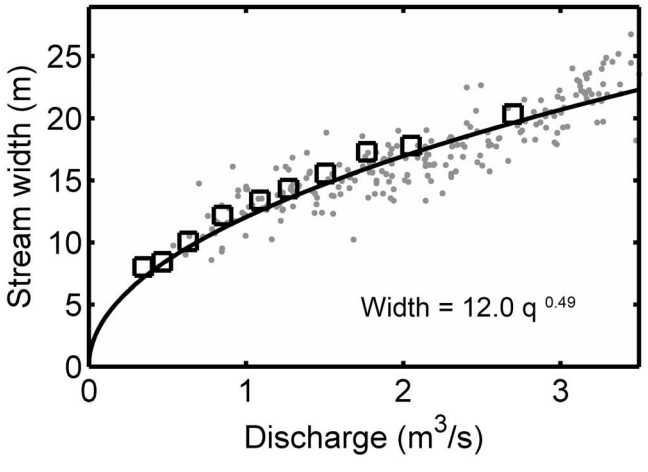

Figure 8. Relationship between stream width and discharge determined with the energy balance model (equation (13)) for the stream reach stretching from site S2 to S4 (gray dots and solid line). Black squares show stream widths inferred from the slope of the relationship between ΔT and Q/q for discrete ranges of discharge (see equation (14) and Figure 7).

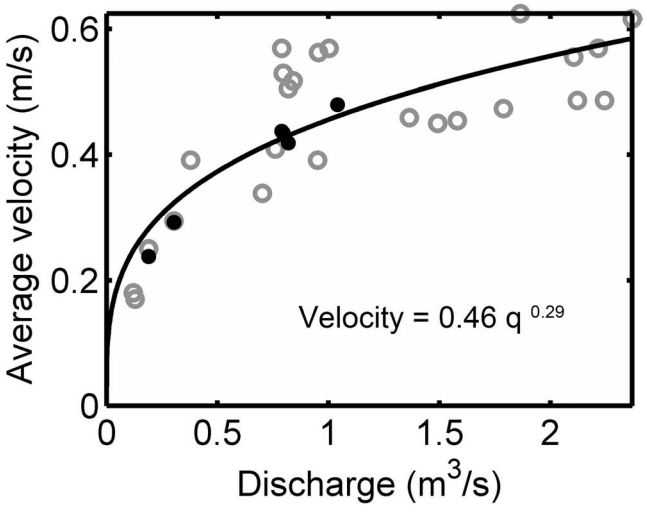

Figure 9. Streamflow velocities measured using dye tracers, with fitted power law hydraulic geometry relationship. Velocities measured over 90 m reach surrounding site S2 (open circles) have greater variability than those measured over the 700 m reach from site S2 to site S7 (solid circles).

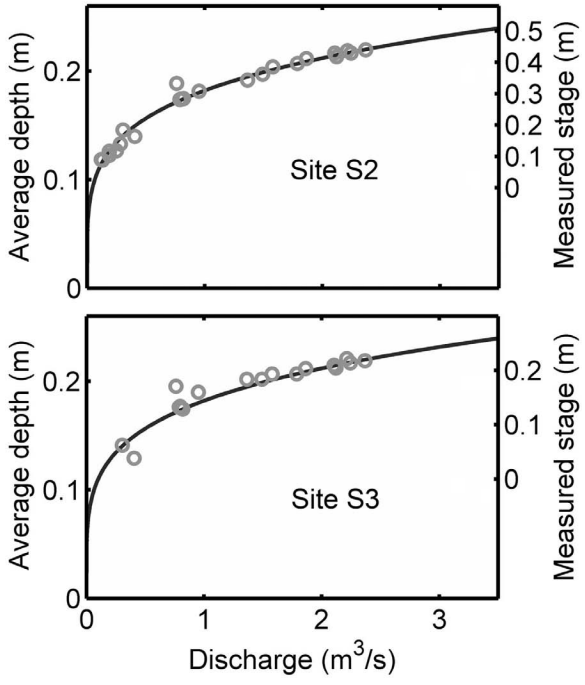

Figure 10. Predicted hydraulic geometry relationship between reach-averaged stream depth and discharge (black curve), compared to stage measurements at two sites along the studied reach (open circles).

upstream reach. The large nighttime temperature increase indicates that heating through the streambed is an important factor warming the water. We think that the most likely explanation for the nighttime temperature increase along the downstream reach is groundwater inflow and hyporheic exchange. First, dye tracers injected into the groundwater monitoring wells at site S5 were detected in small springs on the nearby stream bank after a short time (<20 min), indicating subsurface water flow toward the stream. Second, we do not expect that heat conduction through the streambed could create differences in stream warming between the two reaches as large as those we observe during nighttime.

[41] Groundwater inflows often influence longitudinal stream temperature patterns [*Westhoff et al.*, 2007]. However, the sum of discharges in the two tributaries (at sites S1 and S9) matched the discharge observed below their confluence (at site S7) within the accuracy of the measurements (Figure 3). Thus, if stream-groundwater interactions play an important role across the forefield, any gains and losses of stream water approximately balance between the upstream (sites S2 and S9) and downstream (site S7) discharge measurement sites. On proglacial fields, surface water can often infiltrate into the riparian zone along the streams, and return back to the channels further downstream [*Malard et al.*, 2002], potentially having absorbed additional heat from the riparian subsurface.

5.2. Processes Influencing Stream Warming: Identify Dominant Processes

[42] The stream energy balance equation shows that surface heat fluxes per unit discharge should influence the longitudinal temperature increase along a reach (see equation (1)). To illustrate the relationship between stream water warming, surface heat fluxes and discharge in more detail, we analyzed the results obtained in the beginning of September when snow fell on the glacier resulting in a decrease in discharge (Figure 5). The surface heat fluxes were similar before and after this snowfall but the stream warming suddenly increased because the flowrate $q(t)$ decreased more than the stream surface area, which is given by the (variable) stream width $w(t)$ times the (fixed) reach length L. Thus, not only variations in radiative forcing influence the stream warming, but variations in the hydrological conditions, and in this case discharge variations, play an important role in the stream's temperature dynamics.

[43] With the regression analysis based on the energy balance equation, we can quantify how strongly the surface heat flux per unit discharge influences the stream warming (Figure 6, Table 1). The regression results indicate that heat fluxes across the stream surface are the major cause of

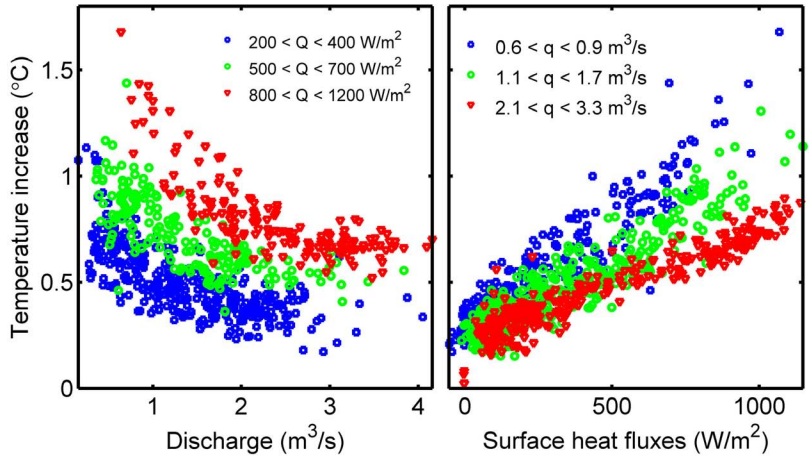

Figure 11. (left) Stream warming as a function of discharge for three distinct ranges of surface heat flux (from S2 to S4, reach length = 330 m), and (right) stream warming as a function of surface heat flux for three distinct ranges of discharge. The longitudinal stream warming shows a strong positive relationship with the surface heat fluxes, but an inverse relationship with stream discharge.

Table 2. Calculated Contribution of Different Heat Sources to the Temperature Increase Between S2 and S4, Averaged Over Daytime, Nighttime, and the Whole Day[a]

Energy Balance Component	Time of Day	Heat Flux (W m^{-2})	Temperature Increase (°C)	Fraction of Heating (%)
Shortwave radiation	Whole day	195	0.16	37
Longwave radiation	Whole day	5	0.00	1
Sensible heat	Whole day	53	0.05	11
Latent heat	Whole day	19	0.02	3
Frictional warming	Whole day	111	0.10	21
Residual heating	Whole day	121	0.12	27
Shortwave radiation	Daytime	327	0.27	50
Longwave radiation	Daytime	7	0.00	1
Sensible heat	Daytime	56	0.05	9
Latent heat	Daytime	21	0.02	2
Frictional warming	Daytime	117	0.10	18
Residual heating	Daytime	120	0.11	20
Shortwave radiation	Nighttime	0	0.00	0
Longwave radiation	Nighttime	2	0.00	0
Sensible heat	Nighttime	49	0.05	16
Latent heat	Nighttime	17	0.01	5
Frictional warming	Nighttime	102	0.10	34
Residual heating	Nighttime	122	0.13	45

[a]Here, daytime was defined as hours with positive solar radiation, and nighttime as hours without sunlight. On average over the monitoring period, solar radiation together with frictional warming and the residual heating component (see text) dominated the energy balance. Note also that the average heat fluxes always were positive, even during nighttime.

the observed temperature increases over three different reaches (S1 to S2; S2 to S3; S3 to S4) including the whole reach stretching from site S2 to S4. We also found that the slopes of the regression lines always became steeper with increasing discharge because the stream width increased with discharge. The differences between the intercepts of the regression lines and the calculated frictional warming were small, and may indicate uncertainties within the calculated surface heat fluxes, measurement errors, or the influence of heat fluxes included in the residual temperature change (see equation (1)). For the downstream reach (S4 to S5), the weak correlation between ΔT and Q/q indicate that surface heat fluxes only weakly influence stream warming, and that one or more of the energy balance terms included in the residual temperature change instead warms the stream water.

[44] To explore the possible role of stream-groundwater interactions in warming the stream between site S4 and S5, we measured groundwater levels, temperatures, and gradients using two monitoring wells, located along a transect perpendicular to the stream (2 and 4 m from the channel) at site S5. Stage measurements 4 m away from the stream were used because the head level differences between the groundwater and stream were more clearly defined in this location than in the near-stream well. Conversely, groundwater temperatures in the near-stream well were used because they better represent the temperature of the subsurface water entering the stream. In the following, we only analyzed observed temperature changes between 21:00 and 06:00 to minimize the influence of radiative fluxes on stream temperature dynamics. We also subtracted the frictional warming constant from the observed stream warming.

[45] The average nighttime temperature increase along the reach stretching from site S4 to S5 correlated well with the head difference between the groundwater and stream level (Figure 12). The weak correlation between variations in air temperature and stream warming indicates that surface heat fluxes do not largely influence the stream temperature dynamics during nighttime. Similarly, the longitudinal increase in stream temperature did not show any obvious relationship with the remaining explanatory variables presented in Figure 12. However, the positive relationship between the temperature increase and the head difference indicates that subsurface inflows influence the stream temperature change.

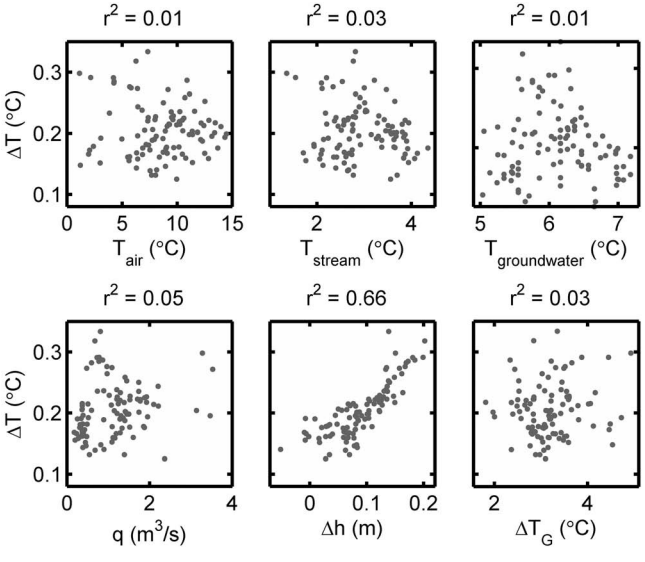

Figure 12. Nighttime average temperature increase (21:00–06:00) from S4 to S5, corrected for frictional warming, compared to several variables that could influence stream warming: air, stream, and groundwater temperatures (T_{air}, T_{stream}, and $T_{groundwater}$, respectively), stream discharge (q), head difference between the stream and a groundwater well 4 m from the channel (Δh), and temperature difference between the stream and a groundwater well 2 m from the channel (ΔT_G). The observed temperature increase shows a clear relationship to the stream-groundwater head difference, but no strong correlation to the other variables.

These subsurface inflows could include groundwater flowing from the surrounding catchment toward the stream, and/or hyporheic return flow of stream water that has infiltrated into the riparian aquifer upstream from the well transect and has been warmed in the subsurface before returning to the channel. We cannot distinguish between these two mechanisms with the measurements that we have.

[46] If subsurface water inflow causes the longitudinal temperature increase, the ratio between observed nighttime stream warming (ΔT) and the temperature difference between the groundwater and stream water (ΔT_G) also gives the ratio between subsurface inflow and stream discharge (provided that groundwater temperatures measured 2 m away from the stream are representative for the inflowing water). We found that a seasonal declining trend in the temperature ratio $\Delta T/\Delta T_G$ (and thus in the ratio of subsurface inflow to streamflow) corresponded to a similar trend in both groundwater level and the head difference between the groundwater and the stream (Figure 13). The seasonally decreasing head difference is a result of a decline in the riparian zone groundwater level. The results indicate that the ratio between subsurface water inflows into the channel and stream discharge is low (roughly 3 to 12%). If other heat fluxes also contribute to the nighttime temperature increase, the calculation above will overestimate the contribution of subsurface inflows to the stream. Note that the heterogeneous sediments and complex topography of the field site lead to highly complex stream and groundwater flow patterns (J. Magnusson et al., submitted, 2012). Therefore, any inferences drawn from our local measurements of head and temperature gradients should be treated with caution. More work is needed to explore the spatial heterogeneity of groundwater levels and stream-groundwater interactions in complex mountainous sites like the Damma glacier forefield.

5.3. Inferring Hydraulic Geometry Relationships From Stream Temperature Measurements

[47] The exponents obtained for the three hydraulic geometry relationships are comparable with observations made elsewhere. The fitted width exponent is toward the upper end of the range usually observed in natural channels [*Park*, 1977]. However, high width exponents are typical for shallow gravel bed streams, as noted by *Smith and Pavelsky* [2008], who found a similar exponent ($b = 0.48 \pm 10\%$) in a remote sensing study of a braided channel in Siberia. In another study, *Chikita et al.* [2010] reported a slightly lower value than ours ($b = 0.42$) for a glacial forefield stream in Alaska. To our knowledge, the highest obtained width exponent ($b = 1.05$) was reported by *Ashmore and Sauks* [2006] for a proglacial braided stream in British Columbia. Our velocity exponent ($m = 0.29$) falls well within the range of values summarized by *Park* [1977]. Our depth exponent ($f = 0.22$) is slightly lower than the majority of observations reported by *Park* [1977], but is higher than the depth exponent reported by *Chikita et al.* [2010] for their proglacial stream ($f = 0.17$). These studies, based on direct measurements, suggest that the exponents derived here may be realistic. Our results indicate that the studied stream reach accommodates discharge mostly through widening rather than large changes in depth and flow velocity.

[48] Note that in the comparison between the reach-averaged depth-discharge relationship and observed stream stage (see Figure 10), the numerical values differ (note the different scales on the left and right axes), which should be expected for at least three reasons: (1) the average depth over an entire reach will generally differ from the average depth at any cross-section, (2) the average depth at any cross-section will be less than the total depth, and will increase more slowly as a function of discharge (because

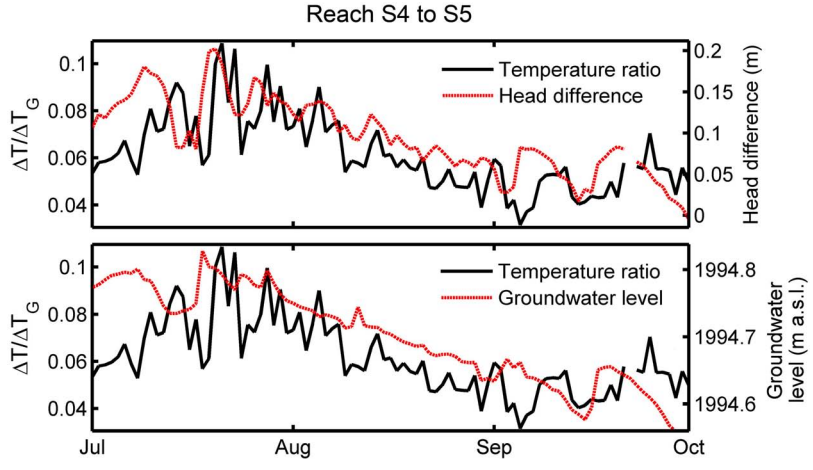

Figure 13. (top) The solid black line shows the ratio between the stream warming (with frictional heating removed) and the stream-groundwater temperature difference ($\Delta T/\Delta T_G$), and the dashed red line shows the head difference between the groundwater level and stream stage. (bottom) The solid line shows the same temperature ratio, but the dashed line shows the groundwater level in the monitoring well (in meters above sea level). The figure shows nighttime averaged values (21:00 to 06:00) for the reach from site S4 to S5. Groundwater levels were measured 4 m from the stream at site S5. The temperature ratio ($\Delta T/\Delta T_G$) declines during the season, and follows the downward trend in groundwater levels in the nearby riparian zone. If subsurface inflows to the channel cause the longitudinal temperature increase, $\Delta T/\Delta T_G$ represents the ratio between subsurface water inflow and stream discharge.

the channel is not rectangular), and (3) there will be a constant offset between total depth and stream stage (because stream stage is measured relative to an arbitrary datum rather than the thalweg elevation). Nevertheless, the stage variations observed at the two sites are consistent with the inferred hydraulic geometry relationship.

[49] Our analysis shows that stream channel geometry has a direct and quantifiable effect on thermal relations in proglacial streams. Stream width has a strong enough effect on stream temperature dynamics (particularly when radiative heat fluxes are large) that the method outlined here can be used to derive reasonable estimates of the relationship between stream width and discharge. Of course, direct measurements of stream width would be preferable to indirect estimates obtained from stream temperature dynamics. However, measuring stream widths can be very difficult in shallow, irregular, highly braided channels like ours, which lack well-defined banks. Furthermore, our method gives estimates of average effective widths over long stream reaches; such estimates are difficult to obtain by most other methods.

5.4. Processes Influencing Stream Warming: Analyzing the Stream Energy Balance

[50] With ongoing glacier retreat, a good understanding of physical processes influencing the stream temperatures in glacial forefields are important, because stream temperatures in these environments are sensitive to changes in climate and runoff regimes, along with changing distances between the streams and the glaciers themselves [*Webb et al.*, 2008; *Chikita et al.*, 2010]. Our results show that variations in stream temperature are inversely related to discharge (Figure 11), which is consistent with previous results from alpine streams [*Constantz*, 1998]. In the case of proglacial streams, however, one might not expect an inverse relationship between discharge and longitudinal warming, because rates of glacial ablation (and therefore discharge) are highest precisely when air temperatures and solar fluxes (and therefore rates of heat transfer at the air-stream interface) are also highest. Our results show that along with surface heat fluxes, stream morphology and discharge variations strongly influence the heating of proglacial streams on the Damma glacier forefield.

[51] We find that solar radiation contributed the greatest to the heat budget of the stream reach between sites S2 and S4 (Table 2). This energy balance component depends only on the albedo of water, which is fairly constant, and the amount of sunlight reaching the stream surface. In steep mountain streams, frictional warming can be large because this heating component is independent of time and discharge and only depends on the down-valley gradient [*Meier et al.*, 2003]. The two energy fluxes mentioned above may not change substantially in the future because they are independent of the water temperature in the stream, which depends largely on the distance to glacier (compare, for example, the temperatures at sites S1 and S9 in Figure 2). On the other hand, the sensible and latent heat fluxes are driven by temperature and vapor pressure gradients above the stream surface. Our data show that the average sensible and latent heat fluxes are positive over the monitoring period, during both daytime and nighttime (Table 2). The calculated latent heat fluxes imply, perhaps surprisingly, that more water vapor condenses on the stream surface (warming the stream) than evaporates from the stream (cooling the stream). This condensation occurs because the air is warm and relatively moist, and the surface of the stream is very cold. With further glacier retreat, the stream temperatures on the field site will likely increase and, at the same time, we might expect drier air with higher temperatures in the future. As a result, we can expect that the latent heat flux will become negative causing water to evaporate from the stream (thus cooling the stream water) instead of condensing. For the particular stream reach from S2 to S4, we cannot identify the processes that underlie the residual temperature increase. This residual heating term is an important component in the stream energy balance, and more work is needed to quantify its possible sources.

[52] In the following, we discuss different uncertainties that may influence our analysis using the energy-balance equation. We are confident in our estimates of net shortwave radiation flux to the water surface; solar flux is measured nearby at the weather station on the forefield, and the albedo of water varies only slightly between different studies [*Chikita et al.*, 2010; *Leach and Moore*, 2010]. We are also confident in our estimates of frictional warming, because they depend only on the elevation difference along the reach (which can be measured precisely), and on the assumption that the available gravitational potential energy is completely dissipated to heat (which is accurate because the change in kinetic energy of the flow is trivial by comparison). The calculated incoming longwave radiation was consistent with measurements made at a weather station located 2.6 km northeast of the forefield and 600 m above it (mean bias of -8 W m^{-2} and root mean square error of 28 W m^{-2}). The calculated turbulent heat fluxes are more uncertain, mainly because the parameters in the equations were determined under conditions different from those prevailing at our study site [see *Webb and Zhang*, 1997; *Leach and More*, 2010]. However, at our alpine study site solar radiation dominates the surface heat fluxes, with relatively small contributions from turbulent heat fluxes. Finally, the measured discharge record at site S2 displayed a root mean square error of 0.10 m^3 s^{-1} compared to the manual discharge observations, where discharges were measured with dilution gauging up to 2.4 m^3 s^{-1}.

[53] The residual temperature change primarily includes heat transport due to groundwater inflow, hyporheic exchange and streambed conduction (see equation (1)). Conductive heat flux through the streambed is negligible in gravel-bedded streams [*Brown*, 1969], and was also assumed negligible in a previous energy-balance study of proglacial streams [*Chikita et al.*, 2010]. This heat flux can be calculated from streambed temperature measurements [*Story et al.*, 2003], but temperature sensors are difficult to install in the stony and heterogeneous sediments that characterize proglacial streambeds. In any case, convection typically transports much more heat than conduction through the hyporheic zone [*Malard et al.*, 2001]. Thus, we think that energy transfer at the streambed interface is probably dominated by heat inputs from groundwater discharge and hyporheic exchange. Some studies suggest that hyporheic flow may store and release heat through the streambed interface and influence the stream temperature dynamics [*Evans and Petts*, 1997; *Alexander and Caissie*, 2003; *Story et al.*, 2003]. *Nielson et al.* [2010] and *Westhoff et al.* [2011] outlined methods for inferring hyporheic

exchange from in-stream temperature observations, and validated their simulation results against independent streambed temperature measurements. Thus, such approaches may be particularly useful for proglacial streams such as ours, but require testing at field sites where validation measurements are possible.

6. Summary and Conclusions

[54] In this study, we measured time series of stream and groundwater temperature, along with groundwater level and discharge, across the Damma glacier forefield in the central Swiss Alps. The seasonal and diurnal patterns observed at the Damma forefield are similar to those observed in other glacierized catchments [*Uehlinger et al.*, 2003; *Brown and Hannah*, 2008]. Our results show that radiative forcing strongly influenced stream temperatures over short distances downstream along the forefield; stream-groundwater interactions also affected the temperature dynamics of some reaches.

[55] By using a simple energy balance equation to interpret the observed longitudinal stream temperature increases, we identified several processes dominating the stream's heat budget. Over three adjacent reaches, heat fluxes across the stream surface and frictional warming largely explained the observed longitudinal increase in stream temperature. Where downstream temperature increases were strongly correlated with radiative forcing, we used the stream energy balance to estimate stream width as a function of discharge. The resulting estimates of stream width were consistent with hydraulic geometry relationships derived by direct measurements in other proglacial streams. Our estimated hydraulic geometry relationships imply that the Damma proglacial stream responds to discharge variations primarily by changing its width, with smaller variations in depth and flow velocity.

[56] The stream warming observed along one reach showed a weak response to meteorological forcing, but still a relatively large temperature increase, likely due to heat exchanges across the streambed interface. By analyzing the nighttime temperature increase along that reach, we found a strong relationship between the hydraulic gradient in the riparian zone and the observed longitudinal stream temperature increase. This observation suggests that gradient-driven subsurface flows into the channel (including hyporheic return flow and/or groundwater inflows) influence the stream warming.

[57] Our results illustrate how detailed studies of proglacial stream temperatures can yield valuable spatially integrated information about hydrological and thermal processes along entire stream reaches. In this study, we used inexpensive and robust sensors that are easily deployable in remote areas such as our study site. However, our results also indicate the potential value of higher-resolution studies of temperature dynamics and heat fluxes in proglacial streams, such as distributed temperature sensing in combination with direct measurements of the energy balance components over the stream surface.

[58] **Acknowledgments.** Financial support for this study was provided by the BigLink project of the Competence Center for Environment and Sustainability (CCES) of the ETH Domain. We thank the many students and staff, particularly B. Fritschi, K. Steiner and F. Herzog, who helped greatly with the fieldwork. The recommendations given by three reviewers improved the manuscript greatly.

References

Alexander, M. D., and D. Caissie (2003), Variability and comparison of hyporheic water temperatures and seepage fluxes in a small Atlantic salmon stream, *Ground Water*, *41*(1), 72–82.

Ashmore, P., and E. Sauks (2006), Prediction of discharge from water surface width in a braided river with implications for at-a-station hydraulic geometry, *Water Resour. Res.*, *42*, W03406, doi:10.1029/2005WR003993.

Becker, M. W., T. Georgian, H. Ambrose, J. Siniscalchi, and K. Fredrick (2004), Estimating flow and flux of ground water discharge using water temperature and velocity, *J. Hydrol.*, *296*(1–4), 221–233.

Brown, G. W. (1969), Predicting temperatures of small streams, *Water Resour. Res.*, *5*(1), 68–75.

Brown, L. E., and D. M. Hannah (2008), Spatial heterogeneity of water temperature across an alpine river basin, *Hydrol. Processes*, *22*(7), 954–967.

Brown, L. E., D. M. Hannah, and A. M. Milner (2006), Hydroclimatological influences on water column and streambed thermal dynamics in an alpine river system, *J. Hydrol.*, *325*(1–4), 1–20.

Cadbury, S. L., D. M. Hannah, A. M. Milner, C. P. Pearson, and L. E. Brown (2008), Stream temperature dynamics within a New Zealand glacierized river basin, *River Res. Appl.*, *24*(1), 68–89.

Caissie, D. (2006), The thermal regime of rivers: a review, *Freshwater Biol.*, *51*(8), 1389–1406.

Campbell, G. S. (1985), *Soil Physics with BASIC: Transport Models for Soil-Plant Systems*, Elsevier, New York.

Chikita, K. A., R. Kaminaga, I. Kudo, T. Wada, and Y. Kim (2010), Parameters determining water temperature of a proglacial stream: The Phelan Creek and the Gulkana Glacier, Alaska, *River Res. Appl.*, *26*(8), 995–1004.

Constantz, J. (1998), Interaction between stream temperature, streamflow, and groundwater exchanges in Alpine streams, *Water Resour. Res.*, *34*(7), 1609–1615.

Dilley, A. C., and D. M. O'Brien (1998), Estimating downward clear sky long-wave irradiance at the surface from screen temperature and precipitable water, *Q. J. R. Meteorol. Soc.*, *124*(549), 1391–1401.

Evans, E. C., and G. E. Petts (1997), Hyporheic temperature patterns within riffles, *Hydrol. Sci. J.*, *42*(2), 199–213.

Flerchinger, G. N., W. Xaio, D. Marks, T. J. Sauer, and Q. Yu (2009), Comparison of algorithms for incoming atmospheric long-wave radiation, *Water Resour. Res.*, *45*, W03423, doi:10.1029/2008WR007394.

Gooseff, M. N., K. Strzepek, and S. C. Chapra (2005), Modeling the potential effects of climate change on water temperature downstream of a shallow reservoir, Lower Madison River, MT, *Clim. Change*, *68*(3), 331–353.

Leach, J. A., and R. D. Moore (2010), Above-stream microclimate and stream surface energy exchanges in a wildfire-disturbed riparian zone, *Hydrol. Processes*, *24*(17), 2369–2381.

Leach, J. A., and R. D. Moore (2011), Stream temperature dynamics in two hydrogeomorphically distinct reaches, *Hydrol. Processes*, *25*(5), 679–690.

Leopold, L. B., and T. Maddock (1953), The hydraulic geometry of stream channels and some physiographic implications, *U.S. Geol. Surv. Prof. Pap. 252*, 56 pp.

Magnusson, J., D. Farinotti, T. Jonas, and M. Bavay (2011), Quantitative evaluation of different hydrological modelling approaches in a partly glacierized Swiss watershed, *Hydrol. Processes*, *25*(13), 2071–2084.

Malard, F., A. Mangin, U. Uehlinger, and J. V. Ward (2001), Thermal heterogeneity in the hyporheic zone of a glacial floodplain, *Can. J. Fisheries Aquat. Sci.*, *58*(7), 1319–1335.

Malard, F., K. Tockner, M. J. Dole-Olivier, and J. V. Ward (2002), A landscape perspective of surface-subsurface hydrological exchanges in river corridors, *Freshwater Biol.*, *47*(4), 621–640.

Meier, W., C. Bonjour, A. Wüest, and P. Reichert (2003), Modeling the effect of water diversion on the temperature of mountain streams, *J. Environ. Eng.*, *129*, 755–764, doi:10.1061/(ASCE)0733-9372(2003)129:8(755).

Neilson, B. T., S. C. Chapra, D. K. Stevens, and C. Bandaragoda (2010), Two-zone transient storage modeling using temperature and solute data with multiobjective calibration: 1. Temperature, *Water Resour. Res.*, *46*, W12520, doi:10.1029/2009WR008756.

O'Driscoll, M. A., and D. R. DeWalle (2006), Stream-air temperature relations to classify stream-ground water interactions in a karst setting, central Pennsylvania, USA, *J. Hydrol.*, *329*(1–2), 140–153.

Park, C. C. (1977), World-wide variations in hydraulic geometry exponents of stream channels—Analysis and some observations, *J. Hydrol.*, *33*(1–2), 133–146.

Ruehl, C., A. T. Fisher, C. Hatch, M. Los Huertos, G. Stemler, and C. Shennan (2006), Differential gauging and tracer tests resolve seepage fluxes in a strongly-losing stream, *J. Hydrol.*, *330*(1–2), 235–248.

Smith, L. C., and T. M. Pavelsky (2008), Estimation of river discharge, propagation speed, and hydraulic geometry from space: Lena River, Siberia, *Water Resour. Res.*, *44*, W03427, doi:10.1029/2007WR006133.

Smith, R. J. (2009), Use and misuse of the reduced major axis for line-fitting, *Am. J. Phys. Anthropol.*, *140*, 476–486.

Stonestrom, D. A., and K. W. Blasch (2003), Determining temperature and thermal properties for heat-based studies of surface-water ground-water interactions, in *Heat as a Tool for Studying the Movement of Ground Water Near Streams, USGS Circ. 1260*, edited D. A. Stonestrom and J. Constantz, pp. 73–80, USGS, Reston, Va.

Story, A., R. D. Moore, and J. S. Macdonald (2003), Stream temperatures in two shaded reaches below cutblocks and logging roads: Downstream cooling linked to subsurface hydrology, *Can. J. For. Res.*, *33*(8), 1383–1396, doi:10.1139/X03-087.

Stull, R. B. (2000), *Meteorology for Scientists and Engineers*, Brooks/Cole, Pacific Groove, Calif.

Uehlinger, U., F. Malard, and J. V. Ward (2003), Thermal patterns in the surface waters of a glacial river corridor (Val Roseg, Switzerland), *Freshwater Biol.*, *48*(2), 284–300.

Unsworth, M. H., and J. L. Monteith (1975), Long-wave radiation at ground. 1. Angular-distribution of incoming radiation, *Q. J. R. Meteorol. Soc.*, *101*(427), 13–24.

Vogt, T., P. Schneider, L. Hahn-Woernle, and O. A. Cirpka (2010), Estimation of seepage rates in a losing stream by means of fiber-optic high-resolution vertical temperature profiling, *J. Hydrol.*, *380*(1–2), 154–164.

Webb, B. W., and Y. Zhang (1997), Spatial and seasonal variability in the components of the river heat budget, *Hydrol. Processes*, *11*(1), 79–101.

Webb, B. W., D. M. Hannah, R. D. Moore, L. E. Brown, and F. Nobilis (2008), Recent advances in stream and river temperature research, *Hydrol. Processes*, *22*(7), 902–918.

Westhoff, M. C., H. H. G. Savenije, W. M. J. Luxemburg, G. S. Stelling, N. C. van de Giesen, and J. S. Selker (2007), A distributed stream temperature model using high resolution temperature observations, *Hydrol. Earth Syst. Sci.*, *11*, 1469–1480.

Westhoff, M. C., M. N. Gooseff, T. A. Bogaard, and H. H. G. Savenije (2011), Quantifying hyporheic exchange at high spatial resolution using natural temperature variations along a first-order stream, *Water Resour. Res.*, *47*, W10508, doi:10.1029/2010WR009767.